Available online at www.sciencedirect.com
SCIENCE DIRECT®
Estuarine, Coastal and Shelf Science 61 (2004) 393–402
ESTUARINE COASTAL AND SHELF SCIENCE
www.elsevier.com/locate/ECSS

Variability of circulation induced by the separation of Gaspe Current in Baie des Chaleurs (Canada): observational studies

Jianping Gan[a,*], R. Grant Ingram[b], Richard J. Greatbatch[c], T. van der Baaren[d]

[a]*Department of Mathematics and Atmospheric, Marine and Coastal Environment (AMCE) program, Hong Kong University of Science and Technology, Clear Water Bay, Kowloon, Hong Kong*
[b]*Department of Earth and Ocean Sciences, University of British Columbia, Vancouver, BC, Canada, V6T 1Z4*
[c]*Department of Oceanography, Dalhousie University, Halifax, NS, Canada, B3H 4J1*
[d]*Bedford Institute of Oceanography, Dartmouth, NS, Canada, B2Y 4A2*

Received 27 October 2003; accepted 16 June 2004

Abstract

The observed variability of summer circulation in the Baie des Chaleurs (BdC, Canada) is found to be largely controlled by the intrusion/separation processes of a coastal jet Gaspe Current (GC) at the bay entrance. An analysis of hydrographic and current meter data showed that the mean counter-wind cyclonic circulation in the BdC from spring to the beginning of the cooling season in 1991 was ascribed to the westward intrusion of the GC. The forcing mechanism of the GC on the BdC was determined by the characteristics of the coastal jet separation. Under the intrusion regime, the GC entered into the BdC along the north coast of the bay, suppressed the local wind-driven eastward currents and formed a cyclonic circulation in the bay. Under the separation regime, GC mainly passed across the entrance of the BdC with the formation of an anticyclonic recirculation at the lee of the jet near the bay entrance and a weaker cyclonic circulation in the bay. Dynamics of the boundary current separation is utilized to reason the observed variability of flow field in the BdC.

Keywords: coastal circulation; jet separation; boundary current; unsteady separation

1. Introduction

The Baie des Chaleurs (BdC) is a semi-enclosed basin with an area of about 35 km by 140 km and an opening to the Gulf of St. Lawrence, Canada (Fig. 1). It is located to the south of the St. Lawrence estuary with the Gaspe Peninsula in between. Near the mouth of the St. Lawrence estuary, upstream inflow and upwelling water from the northwestern Gulf generate a jet-like feature known as the Gaspe Current (hereafter called GC) (Fig. 1). The GC can have speed up to 100 cm s^{-1} and is mainly found in the upper 100 m of the water column (Tang, 1980; Bugden, 1981; Benoit et al., 1985).

The southward moving GC along the Gaspe Peninsula can separate from the coastal boundary at the entrance of the BdC (Gan et al., 1997). Current separation in the ocean has been observed in numerous locations. The Gulf Stream separation from the North American coast at Cape Hatteras as it moves northward is a typical example. Wang (1987), using numerical experiments with a density current in a strait showed the formation of an anticyclonic eddy at the exit of the strait during current separation. Signell and Gyer (1991),

* Corresponding author.
E-mail address: magan@ust.hk (J. Gan).

0272-7714/$ - see front matter
doi:10.1016/j.ecss.2004.06.009

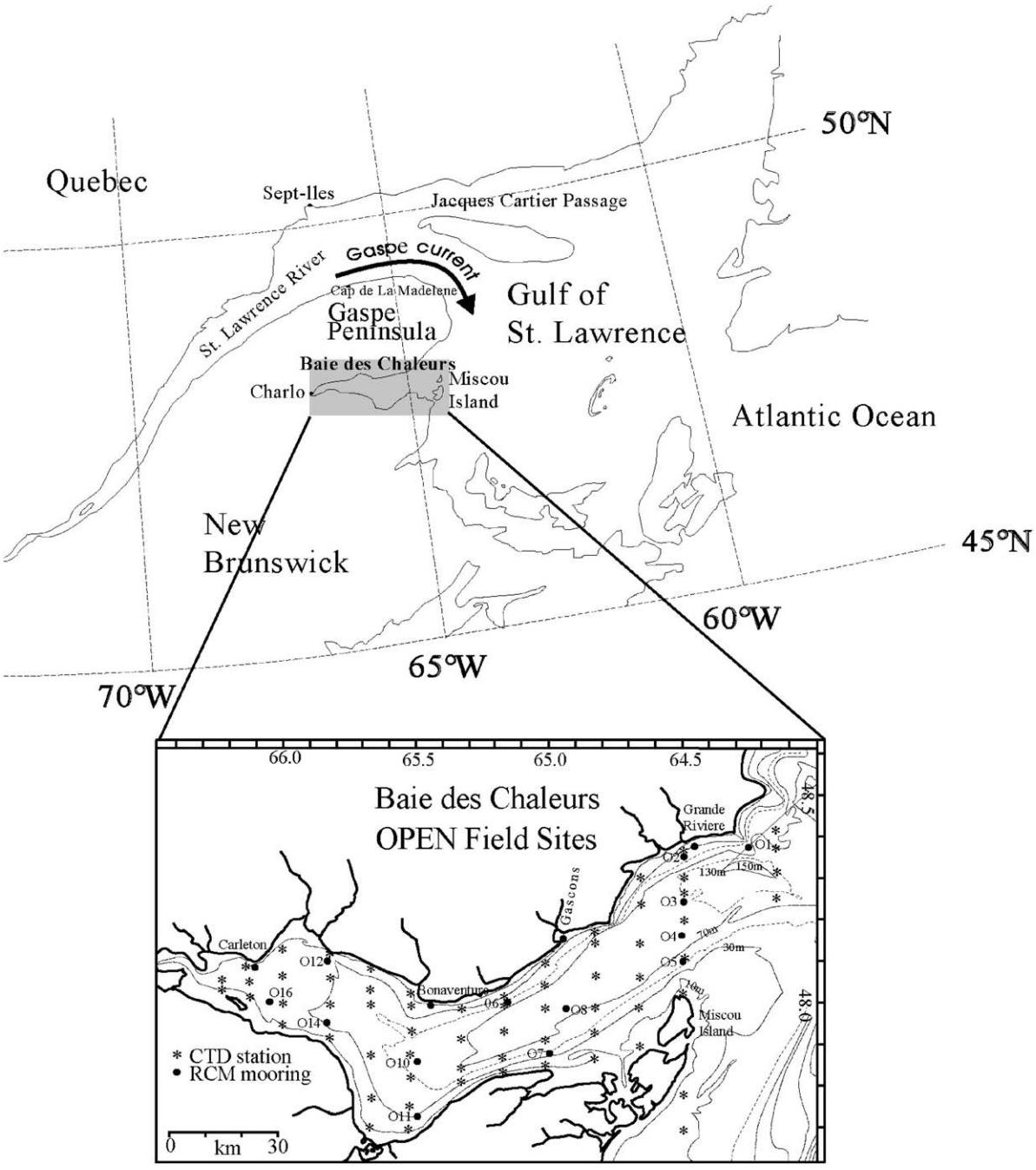

Fig. 1. Geographic locations of the Gulf of St. Lawrence and the Baie des Chaleurs, Canada (upper panel) and bathymetry, current meter moorings and CTD profiles in 1990 and 1991 (lower panel). Black circles adjacent to the north shore are designated by the nearest village name.

based on a dynamical analysis demonstrated that flow separation occurs when the pressure gradient force (PGF) along the boundary switches from favoring to adverse (against the flow). Gan et al. (1997) analyzed the dynamical process involved in an unsteady jet separation. They found that the separation is related to an adverse ageostrophic PGF (APGF) and the deceleration of the jet has significant impact on the separation. Based on the dynamics of the boundary current separation (Batchelor, 1967), the separated GC is expected to overshoot the eastern tip of the Gaspe Peninsula and pass across the entrance of the bay without intruding into the BdC. An anticyclonic recirculation eddy can be formed in the separated GC. After separation, the GC can change its path, flow northwestward following the flow in the recirculation and reattach to the coast near the bay entrance (called reattachment). In the case of no separation, the GC can turn around the eastern tip of the Gaspe Peninsula, maintain its path along the coastline and intrude into the bay.

There have been only a few studies on dynamical variability of circulation in the BdC, especially regarding the effect of the GC separation. Bonardelli et al. (1993) discussed the current and temperature variability along the north shore of the BdC. They found a strong seasonal signal in the cyclonic circulation pattern near the surface in the BdC and suggested that the intrusion from the GC was responsible for the westward flow along the north shore of the BdC in the summer. The influence of the GC on the bay was also mentioned by Filteau and Tremblay (1953), and by Lauzier and Marcotte (1965) based on the limited observation data. The observed features of the influence from GC intrusion/separation on the BdC were not identified in these studies. The model results from Gan et al. (1997) suggested that the variability of circulation pattern in the BdC was mainly controlled by the unsteady GC intrusion/separation processes. Observational evidences of these processes are presented in this paper.

2. Data

A major data collection program was conducted in the BdC during the period 1991–1993, as part of the Ocean Production Enhancement Network (OPEN) program. The main objectives of that study were to understand the nature and variability of the physical processes acting in the bay and their influence on biological productivity. From June to November 1990, 27 Aanderaa RCM 4S and RCM 7 instruments were moored at 11 locations (station O1, stations O3–O11 and station Bonaventure) in the BdC (Fig. 1). During the same period in 1991, 36 instruments were moored at 18 locations in the bay. The mooring sites in 1991 included the locations used in 1990 and are shown in Fig. 1. The sampling interval was 30 min for all deployments. The velocity vectors were decomposed into U and V components with positive U and V components directed eastward and northward, respectively. Due to fouling and other problems, records were truncated at some stations. In the discussion of the monthly mean fields, time series with fewer than 20 days of data in any month are not included. Several CTD profile transects were taken along the longitude of every moored current meter during the study period from June to October 1991 using a Seacat SBE 19 (Fig. 1). A time series of the meteorology variables, obtained from the Charlo station (Fig. 1), is presented in Fig. 2a. It shows the prevailing westerly in BdC in 1990 with maximum air temperature in August. The wind measurement in BdC is not available for 1991. Data from Cap de le Madeleine north of Gaspe Peninsula (Fig. 1), however, indicate that eastward winds were dominant in summer 1991 (Fig. 2b). The mean currents and their statistical characteristics in 1991 are listed in Table 1. Most of the resultant velocity components were considered significantly different from zero ($p < 0.05$). Generally large standard deviations (σ) in the current velocities at all mooring stations suggest strong variability in the flow field. The mean westward and eastward u is found at the stations close to the north (O2, O6, B7 and O7) and south (O7 and O5) shore, respectively. In addition, the mean and the associated σ of the east–west velocity component u are larger than those of the north–south velocity component v in almost all the stations. These statistical features indicate a mean cyclonic circulation pattern with strong temporal variability in the BdC during the observation period.

3. Mean circulation and its variability

3.1. Mean flow fields

The monthly mean flow fields in the BdC obtained from the current meter measurements in 1991 are presented in this section to describe the variability of the circulation in the bay. Fig. 3a–d show the mean cyclonic circulation pattern in the BdC from June to September 1991. The circulation driven by the prevailing westerly wind (Fig. 2b) during this period was expected to form eastward geostrophic currents on the north coast of the bay as a result of an across-shore pressure gradient from wind-driven upwelling. The observed counter-wind westward currents on the north coast and the corresponding cyclonic circulation in the BdC must therefore be driven by a forcing opposite to the prevailing eastward wind stress. Evidently, the westward inflows from the GC intrusion along the north coast of the BdC lead to the formation of the cyclonic circulation in the bay by suppressing local wind-driven eastward currents. Over the four months of the study, the upper level currents were northwestward (or westward) at O3 near the north shore and eastward at O5 near the south shore. These observations suggest that GC entered and exited the BdC from O3 and O5, respectively. The currents at O1 near the entrance of the bay would be negative (westward) if the GC were in the intrusion regime. The observed eastward (or south-eastward at depth) currents at O1, however, demonstrate that the GC did not directly enter the BdC by attaching to the northern coast of the BdC as it moved southward along the coastline of the Gaspe Peninsula. Instead, it separated from the coast near O1 and subsequently entered the bay near O3 as indicated by the velocities at O1, O2 and O3.

After entering the bay, the currents reattached to the north coast at O2 and bifurcated there in June and July. The shifting of velocity at O2 from the northwestward in June to mainly northeastward in July is most likely caused by the east–west movement of the recirculation eddy. Mainly westward currents at O3 and weaker

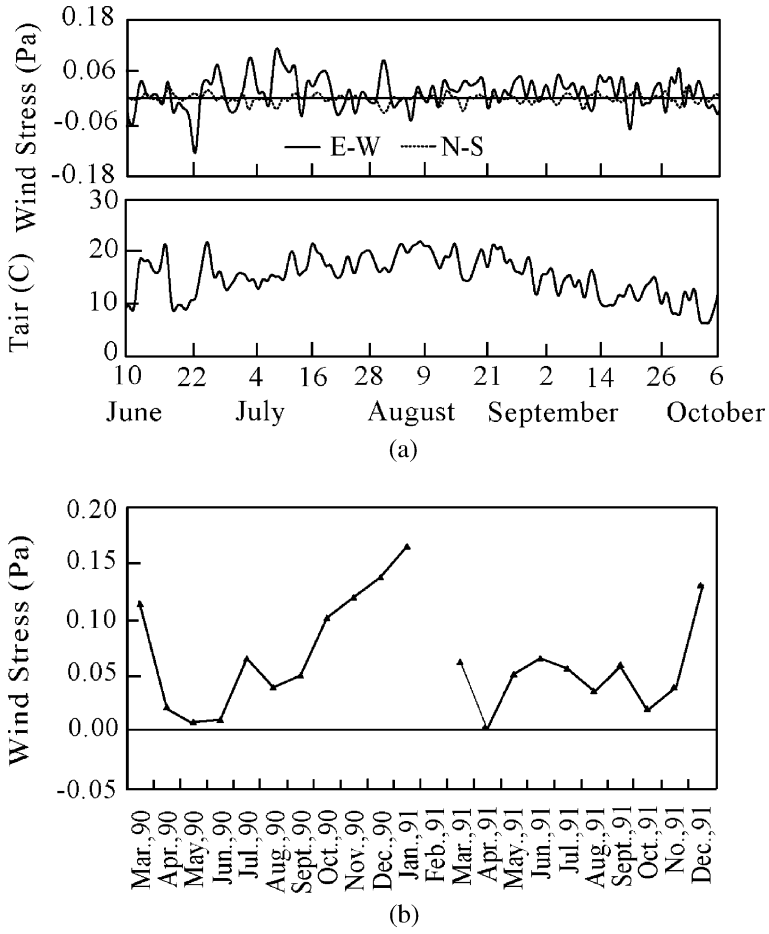

Fig. 2. (a) Time series of wind stress (Pa) and air temperature (°C) at the Charlo station in 1990. Positive E–W and N–S values refer to the eastward and northward wind stress, respectively; (b) time series of monthly east–west wind stress (Pa) at Cap de la Madeleine north of the Gaspe Peninsula.

eastward/northward currents at O1/O2 in August and September indicate a weaker anticyclonic recirculation in the region. West of the bay entrance at O8, the observed currents exhibited a complex circulation structure. Although the spatial resolution of the current meter moorings near station O8 was not adequate to identify the circulation pattern there, supporting evidences from modeling result (Fig. 4) and the mixed layer depth (MLD) fields calculated from CTD observations in the bay (see Section 3.2) suggest that the northward or southward currents at O8 in June and July indeed reflect cyclonic eddy in this area. The modeling results in Fig. 4 are obtained from a 2.5-layer model with primitive equation dynamics and an embedded bulk MLD model (Gan et al., 1997). Realistic atmospheric fluxes were used as model forcing. Depending on the magnitude of the GC transport, as well as the rate and duration of GC deceleration or acceleration, GC can be separated or non-separated, which lead to the formation of two different circulation patterns as shown in Fig. 4. Strong GC with long duration of deceleration is likely to separate (Fig. 4a) and the GC with the opposite conditions will lead to the intrusion without separation (Fig. 4b). In both conditions, a cyclonic eddy forms near O8. The east–west shifting of this eddy lead to the change in the velocity direction at the station from June to July. In the central and western parts of the bay, the westward and eastward currents at the stations located near the north and south shores, respectively, demonstrated the features of cyclonic circulation during the entire observation period.

The intensity of the GC separation, which is inversely correlated with the strength of the GC intrusion into the BdC, can be estimated by measuring the strength of the vorticity in anticyclonic recirculation at the lee of the separated GC. The vorticity is defined as

$$\zeta = \frac{\partial v}{\partial x} - \frac{\partial u}{\partial y}, \tag{1}$$

where u and v are the velocities in the x and y coordinates with positive x directed to the alongshore direction (38° counter-clockwise from the true east,

Table 1
Monthly mean ($\bar{x}$), standard deviations (σ) and error (ε) of mean (U m s^{-1}) and (V cm s^{-1}) components at different depths (m) for June, July, August and September, 1991

D	u, v	June			July			August			September		
		$\bar{x}$	σ	ε	$\bar{x}$	σ	ε	$\bar{x}$	σ	ε	$\bar{x}$	σ	ε
STA.O1													
20 m	u	7.20	33.5	0.19	8.11	24.93	0.65	−0.42	22.07	0.57[a]			
	v	−5.93	14.61	0.44	−2.83	10.0	0.39	0.79	10.72	0.28			
30 m	u	9.71	30.62	0.92	3.76	21.13	0.36	4.16	18.98	0.34	4.65	20.41	0.54
	v	−3.15	15.04	0.45	−2.14	13.85	0.36	2.47	13.17	0.34	1.25	11.36	0.30
55 m	u	1.74	9.64	0.29	0.59	9.27	0.24	1.68	6.99	0.18	1.63	8.67	0.23
	v	−7.36	15.16	0.45	−6.07	15.60	0.40	−7.19	16.03	0.42	−8.11	16.02	0.42
STA.O2													
20 m	u	−7.82	19.34	0.58	5.74	20.33	9.53	−0.03	15.73	0.41			
	v	1.12	11.97	0.36	6.41	13.54	0.35	1.15	8.9	0.23			
30 m	u	−4.69	13.68	0.49	5.16	20.28	0.53	−2.16	16.39	0.43			
	v	3.31	10.28	0.31	6.12	12.64	0.33	2.39	11.33	0.29			
STA.O3													
25 m	u	−3.71	21.33	0.64	−12.4	20.92	0.54	−6.49	21.28	0.55	−8.6	17.03	0.45
	v	1.58	14.36	0.43	7.95	15.23	0.40	−4.31	12.23	0.32	−3.05	10.03	0.26
50 m	u	−5.01	12.74	0.38	−1.67	13.3	0.35	−3.02	12.86	0.33	−1.28	14.27	0.38
	v	4.27	10.82	0.32	1.39	11.54	0.30	−0.15	11.08	0.29[a]	1.05	8.67	0.23
90 m	u	−0.52	11.87	0.35[a]	1.16	10.96	0.28	−0.15	9.00	0.23[a]			
	v	0.15	14.18	0.42[a]	−1.17	13.53	0.35	−2.18	15.12	0.39			
STA.O4													
55 m	u	2.22	14.85	0.44	−0.66	10.92	0.53[a]	1.78	11.02	0.29	0.88	9.29	0.25
	v	2.18	18.08	0.54	1.22	17.86	0.46	0.25	17.72	0.46[a]	1.30	17.77	0.47
STA.O5													
20 m	u	6.97	23.16	0.69	11.02	21.28	9.55	12.14	20.01	0.52	14.91	20.71	0.55
	v	−0.65	10.03	0.3	3.24	9.57	0.25	2.31	8.75	0.23	3.73	7.91	0.21
35 m	u	1.41	13.74	0.41	0.39	11.48	0.30[a]	2.3	13.07	0.34	3.52	11.91	0.31
	v	1.57	14.96	0.45	0.26	16.02	0.42[a]	0.68	15.75	0.41[a]	0.53	13.39	0.35
STA.O6													
35 m	u	−7.01	17.75	0.54	−7.81	16.66	0.43	−7.08	19.73	0.51	−8.79	21.94	0.58
	v	−1.23	6.67	0.2	−0.98	4.66	0.12	−0.63	5.51	0.14	−1.69	6.71	0.17
STA.O7													
16 m	u	3.42	16.26	0.49	7.53	15.66	0.41	2.71	12.62	0.33			
	v	1.05	7.32	0.22	0.29	6.36	0.17[a]	0.25	5.43	0.14[a]			
32 m	u	3.38	14.44	0.44	0.5	14.49	0.38[a]	−0.81	16.9	0.44[a]			
	v	0.63	5.18	0.16	−0.38	4.1	0.11	−0.38	4.56	0.12			
STA.O8													
20 m	u	−2.01	19.08	0.57	−2.72	17.86	0.46	−4.72	15.26	0.40	−7.05	14.11	0.27
	v	2.27	12.32	0.37	−7.9	17.12	0.44	−0.99	12.15	0.32	3.52	8.76	0.23
31 m	u	−0.49	15.25	0.45[a]	−0.21	14.55	0.38[a]	−2.29	14.08	0.37	−8.85	16.25	0.43
	v	3.01	11.73	0.35	−6.7	15.11	0.39	−0.84	12.18	0.32	2.96	11.52	0.30
55 m	u	2.43	12.57	0.37	0.22	11.86	0.31[a]	−0.14	12.14	0.32[a]	0.48	10.15	0.27[a]
	v	3.09	13.06	0.39	−1.08	9.26	0.24	−0.38	10.95	0.28[a]	0.22	9.79	0.26[a]
STA.O10													
16 m	u	−4.5	16.35	0.51	−3.81	20.68	0.54	2.45	14.98	0.09	−3.36	16.29	0.13
	v	−3.78	14.81	0.46	−0.59	13.11	0.34[a]	−5.0	11.48	0.30	−5.62	9.66	0.26
STA.O12													
15 m	u	−5.26	4.34	0.14	−5.8	4.44	0.12	−4.03	3.45	0.09	−5.22	4.79	0.13
	v	−1.4	1.47	0.05	−2.16	1.84	0.05	−1.37	1.41	0.04	−1.21	1.37	0.04
B													
7 m	u	−5.79	21.81	0.58	−2.18	18.41	0.48	−9.14	20.62	0.54	−0.16	17.71	0.47[a]
	v	0.04	6.17	0.16[a]	0.12	5.04	0.13[a]	1.04	4.98	0.13	0.83	4.54	0.12
C													
7 m	u	−11.18	12.58	0.33	−10.84	11.44	0.30	−10.88	12.64	0.33	−13.11	11.56	0.31
	v	−3.07	7.55	0.20	−3.43	6.59	0.17	−3.53	8.1	0.21	−3.69	6.7	0.17

(*continued on next page*)

Table 1 (*continued*)

D	u, v	June			July			August			September		
		$\bar{x}$	σ	ε	$\bar{x}$	σ	ε	$\bar{x}$	σ	ε	$\bar{x}$	σ	ε
G													
20 m	u	−2.24	8.36	0.22	−2.55	7.74	0.20	−2.88	6.26	0.16	−1.9	6.65	0.18
	v	−0.6	5.6	0.15	−0.7	3.81	0.10	−0.59	3.74	0.01	−0.62	4.38	0.12
GA													
20 m	u	−4.31	7.76	0.21	−3.61	6.84	0.18	−1.84	4.98	0.129			
	v	−4.21	7.06	0.19	−3.58	5.68	0.15	−1.7	4.33	0.11			

The 'B' and 'C' stand for the Bonaventure and Carleton, respectively. 'G' refers to Grande Riviere station and 'GA' to Gascons station. The locations of stations are shown in Fig. 1. The standard deviation $\sigma = [1/(n-1)\sum(X_i - \bar{x})^2]^{0.5}$; the error $\varepsilon = \sigma/n^{0.5}$.

[a] Indicates not significantly different from 0 at 95% confidence level.

Fig. 3a) and positive y to the across-shore direction, respectively. The alongshore direction (x) is chosen to be close to the orientation of the coastline between stations Grande Riviere and O6. Based on this coordinate, the vorticity of the anticyclonic recirculation off Grand Riviere (west of O1) can be estimated by the velocities between O1 and O3, which are aligned in the x direction. The observed velocities (U, V) at 25 m are rotated 38° anticlockwise to (u, v) in order to obtain vorticity from Eq. (1). In August and September, velocities from depth 30 m are used for the vorticity calculation. The results show that the vorticity of recirculation strengthened from June ($-0.5 \times 10^{-5}\ s^{-1}$) to July ($-0.8 \times 10^{-5}\ s^{-1}$), and weakened in August ($-0.5 \times 10^{-6}\ s^{-1}$) and September ($-0.2 \times 10^{-5}\ s^{-1}$). Clearly, the GC separation intensified from June to July and weakened in August. This finding can also be supported by the weaker westward currents at Bonaventure in June and July as will be presented in Section 4.

3.2. The mixed layer depth

To further identify the circulation pattern in the BdC during the upwelling season, hydrographic data from

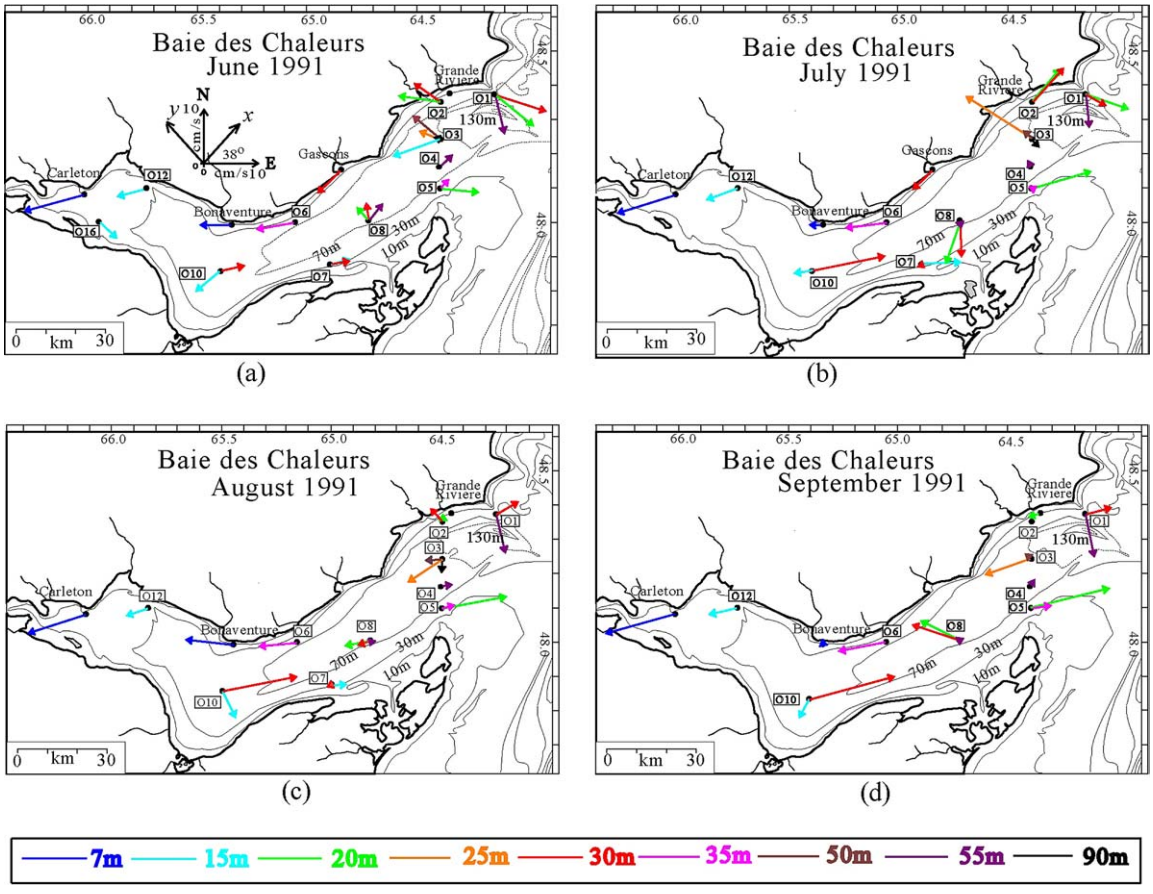

Fig. 3. Mean circulation in (a) June, (b) July, (c) August and (d) September in 1991. The mooring depths of the current meters are shown by different colors.

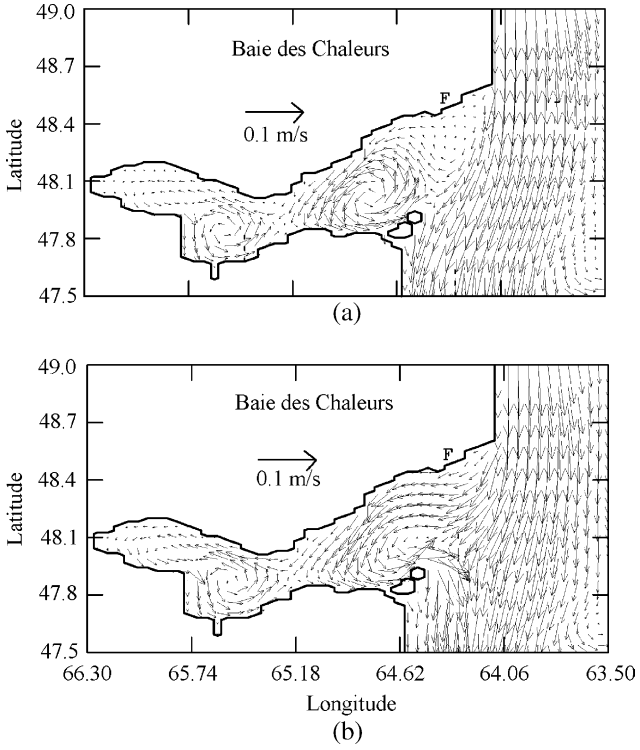

Fig. 4. Two possible mean circulation patterns in the mixed layer in September 1990 for (a) GC separation and reattachment and (b) GC intrusion, depending on the magnitude of the GC transport, as well as its rate and duration of deceleration or acceleration. The current speed in the figure is truncated at 0.1 m s^{-1} (adapted from Gan et al., 1997).

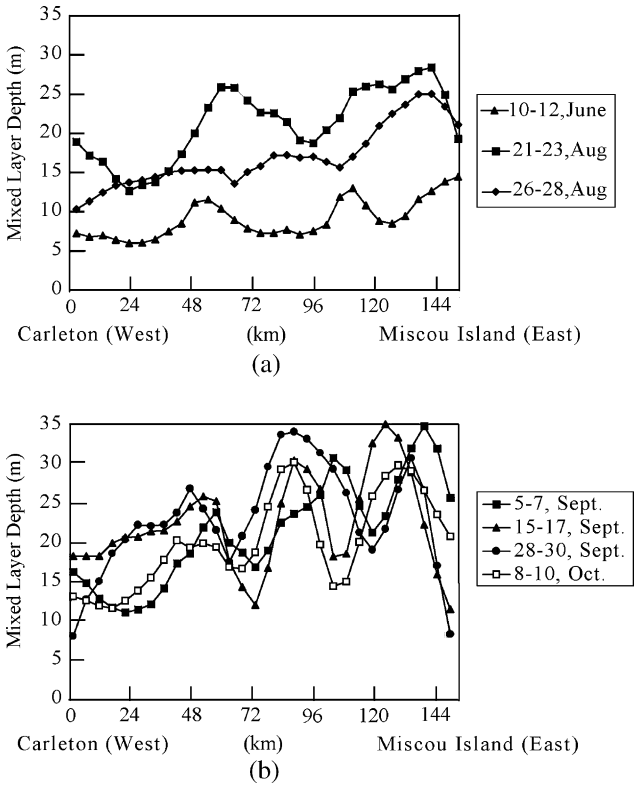

Fig. 5. Mean mixed layer depth from instantaneous CTD profiles in 1991 for (a) June and August, (b) September and October. The horizontal axis is the distance from Carleton to Miscou Island along E–W axis in the central part of the bay.

the CTD cruise are analyzed. In a two-layer system, the spatial gradient of the mixed layer depth (MLD) directly reflects the pressure gradient field of circulation and is useful in identifying the flow fields. Fig. 5a and b show the MLD derived from the CTD cruises in 1991. The MLD was averaged along each CTD longitude section of every current meter mooring and plotted along the E–W axis in the central part of the bay. We define the MLD to be the upper-ocean layer whose depth averaged temperature is a ΔT value higher than the water temperature just below. Based on the observed density profiles and approximation of a two-layer system (Gan et al., 1995), ΔT is determined to be 3 °C in this study.

Factors controlling the MLD can be seen from the continuity equation for the mixed layer,

$$\frac{\partial h}{\partial t} = -\nabla(hV) + W_e, \tag{2}$$

where h is the MLD, t is time and V is the horizontal velocity vector at the mixed layer. W_e is the entrainment velocity, which is governed by the balance between the surface buoyancy flux and mixing due to wind- and buoyancy-generated turbulence. $-\nabla(hV)$ is the convergence of the flow field. From June 10 to 12, an MLD of less than 15 m was found along the bay from Carleton to Miscou Island (Fig. 5a). It deepened in August, with the largest MLD of about 30 m located at the entrance of the bay. In September, the MLD was about 15 m near Carleton and over 30 m at the entrance of the bay (Fig. 5b). Deepening of the MLD from June towards September is clearly shown in Fig. 5.

According to Eq. (1), $\partial h/\partial t$ is subject to the control of W_e and $-\nabla(hV)$. From June to August, stronger atmospheric heating and weaker wind (Fig. 2) result in a smaller W_e, while cooling of the surface water and increasing of the wind magnitude from September onwards have the opposite effect, and result in a positive contribution to $\partial h/\partial t$ from W_e. Accordingly, a deeper MLD is expected in September and October as shown in Fig. 5. In addition, convergence $\nabla(hV) > 0$ due to the westward intrusion of GC can dynamically deepen h, particularly at the entrance of the bay (Gan et al., 1996).

The pattern of spatial variation in the MLD in Fig. 5 is consistent with the circulation structure discussed in the mean flow fields. Three MLD troughs (shallower MLDs) along the E–W axis of the bay suggest the existence of cyclonic eddies at the entrance, center and western parts of the bay (Fig. 3). These eddies had horizontal scales of about 30–40 km and were not completely resolved by the data from the current meter

moorings, but were shown in the modeling result (Fig. 4). A much deeper MLD and the consequently stronger eddies in September corresponds to the strengthening of the GC intrusion during this period as indicated by the analysis from the mean flow fields.

4. Discussion

The field observations indicate that cyclonic circulation in the BdC is formed by the intrusion of the GC. The strength of the GC intrusion is greatly reduced when the GC separates. Since the GC intrusion/separation occurs at the bay entrance, local circulation is mainly controlled by the flow field associated with the intrusion/separation processes and is also crucial to the circulation inside the bay. It appears that understanding the dynamical mechanism of the GC intrusion/separation processes is essential in determining whether the GC intrudes or separates at the entrance of the BdC.

Results from most previous studies (e.g., Batchelor, 1967; Signell and Gyer, 1991; Gan et al., 1997), suggest that separation of a highly nonlinear boundary current is associated with an adverse, along-boundary PGF. Recently, Gan and Allen (2002) showed that an adverse APGF was responsible for a coastal jet separation near a cape. It is informative to describe the relation between the adverse PGF and separation of the GC by considering a simplified steady x-component of the momentum equation close to the boundary. The northeast–southwest (NE–SW) oriented coastline downstream of salient edge (location F in Fig. 4) near the entrance of the BdC is chosen since the GC is likely to separate from the coast there.

$$-fv+u\frac{\partial u}{\partial x}+v\frac{\partial u}{\partial y}=-\rho^{-1}\frac{\partial p}{\partial x}+K\left(\frac{\partial^2 u}{\partial x^2}+\frac{\partial^2 u}{\partial y^2}\right), \tag{3}$$

where u and v are the velocity in the alongshore (x) and across-shore directions (y), respectively. The definition of coordinates (x,y) can be seen in Section 3.1 and Fig. 3a. ρ is the water density; f is Coriolis parameter; p is the pressure and K is the horizontal eddy viscosity coefficient. The bottom friction is assumed to be small as compared to the horizontal eddy viscosity in the upper ocean where the GC is located. With the continuity equation,

$$\frac{\partial u}{\partial x}+\frac{\partial v}{\partial y}=0, \tag{4}$$

and with no-slip boundary condition ($u=0$, $v=0$) at the wall ($y=0$) along the coastline near F, the APGF from Eq. (3) can be written as

$$\mathrm{APGF}=fv-\rho^{-1}\frac{\partial p}{\partial x}=-K\frac{\partial^2 u}{\partial y^2}. \tag{5}$$

It can also be shown from Eq. (1), Eq. (4) and the no-slip condition at the wall that the across-shore vorticity gradient at the no-slip wall is

$$\frac{\partial \varsigma}{\partial y}=-\frac{\partial^2 u}{\partial y^2}. \tag{6}$$

By combining Eq. (5) and Eq. (6), we have

$$\mathrm{APGF}=K\frac{\partial \varsigma}{\partial y}. \tag{7}$$

The negative vorticity generated by the velocity shear between the GC and the no-slip NE–SW oriented coastline downstream of salient edge is decreasing offshore (southward) as the vorticity gradient is diffused down by the eddy viscosity close to the wall. In another word, positive ζ is introduced into a flow of predominantly negative ζ thus requires a region on the wall over which $\partial\zeta/\partial y$ is positive. According to Eq. (7), it may lead to the generation of an adverse (positive x direction) APGF opposite to the southwestward GC along the coastline near the salient edge. With the formation of reverse APGF, the corresponding reverse current (eastward) and vorticity (positive) are formed close to the boundary of the coastline (Gan et al., 1997). It should be noted that Eq. (5) is not a general relationship applying throughout Gaspe Current but one that applies specially to illustrate the mechanism of separation at a wall as a result of the no-slip boundary condition. Eq. (7) is a necessary condition for GC to separate. Whether diffusion of positive ζ into the flow forms adverse vorticity ($\zeta>0$) depends on whether this diffusion is more than counterbalances diffusion and/or advection from the negative vorticity between the core of the GC and coastline. For an unsteady condition, the dynamical process of separation is much more complex. The temporal variation in the unsteady GC can modify the magnitude of the adverse APGF. There has been little study in the unsteady jet separation in the ocean. Gan et al. (1997) found, as shown in Fig. 4, that a deceleration in a weakening GC could enhance its separation, which is likely dissipated during the phase of acceleration. Using a simple box model and historical data from 1947 to 1974, Bugden (1981) found that the GC transport decreased during the spring, reached a minimum value in the summer, and then increased towards the winter. The deceleration in a weakening GC in June and July and the acceleration in a strengthening GC in August and September suggest that the GC was likely to be in the separation and intrusion regimes in these two periods, respectively.

The separation of a coastal boundary current is also associated with eddy generations caused by the nature of GC at the entrance of the bay (recirculation eddy) and by the resulting strength of the GC intrusion (eddies in the BdC). To aid in the discussion and illustration of the relation between observed eddies in the bay and GC intrusion/separation, the characteristic BdC eddies are summarized in the schematic diagram (Fig. 6). Eddy C_1 in Fig. 6a was the result of a recirculation eddy from the GC separation. Eddy C_2 was formed by the combined effects from the westward currents due to GC intrusion along the north coast and the wind-driven eastward currents on the south coast. In the central and western parts of the bay, the observed cyclonic eddies, C_3 and C_4, were driven by the westward intrusive currents. The intrusion of the GC can occur either by attachment or by reattachment according to the nature of GC at the entrance of the bay. During the attachment (Fig. 6b), GC enters the bay along the north coast of the bay and its stronger westward flow could then intensify the C_2, C_3 and C_4. During the reattachment (i.e. the separated GC reattaches to the coastline, Fig. 6a), the westward currents contributed by the GC to eddy C_2, C_3 and C_4 were much smaller since part of the GC reattached to the coast is recirculated out of the bay by the C_1. If GC experiences both separation and attachment during the data collection period, the pattern shown in Fig. 6a is expected in the monthly mean field as long as the separated GC is dominant. Circulation patterns associated with the separated and non-separated GC in Fig. 6 are also found in the numerical experiments (Fig. 4), which suggested that separation or intrusion occurrence depends on the magnitude of the GC transport, as well as on its rate and duration of deceleration and acceleration (Gan et al., 1997).

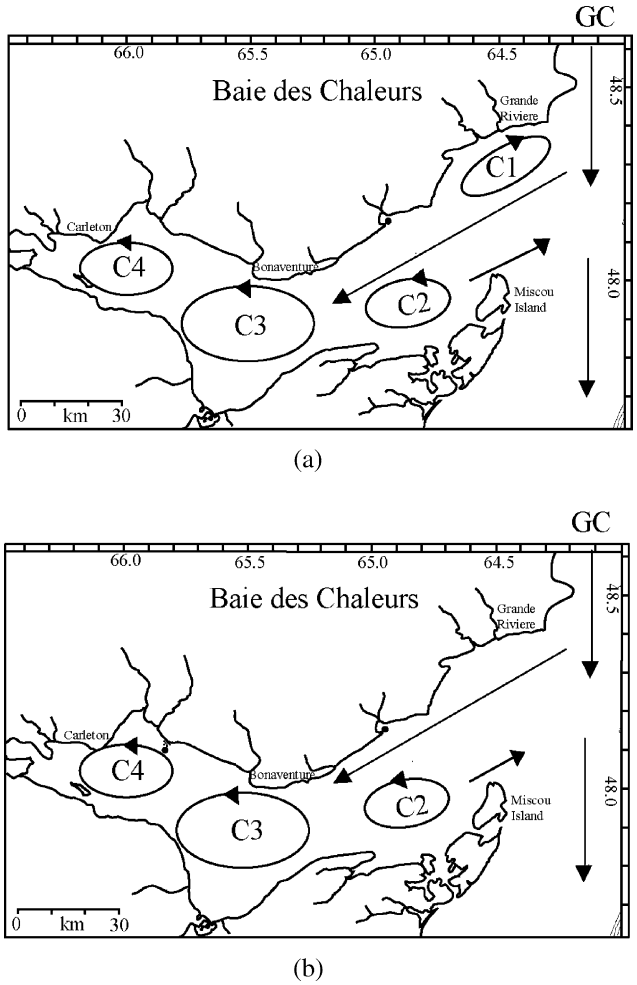

Fig. 6. Sketch showing possible eddy distribution in BdC for (a) GC separation and reattachment; and (b) GC intrusion without separation.

The variability of the circulation in the bay was, thus, altered by the variability in the separation/intrusion processes. In June 1991, the mean circulation (Fig. 3a) followed a pattern similar to Fig. 6a. Time series of 36 h low-pass filtering u at O1 showed the existence of both westward and eastward currents (Fig. 7) during the measurement period, but with stronger eastward currents. Since the currents at O1 were directly related to the strength of the recirculation from the separated GC, the results in Fig. 7 suggest that the mean circulation in June (Fig. 3a) was the sum of non-separated (Fig. 6b) and separated patterns (Fig. 6a) and was dominated by the separated pattern. The mean intensity of C_2 was strong due to the fact that the circulation pattern near this location was consistently cyclonic in both the separated and non-separated GC. In a similar analysis, the intensified vorticity in recirculation C_1 (see Section 3) and mainly eastward currents at O1 (Fig. 7) imply that the GC is primarily in the separation regime in July. By definition, strong separation will prevent the GC from directly entering the bay along the north shore. With dominant separation of the GC in June and July, the GC mainly passed across the entrance of the bay and intensified the C_1 and C_2 near the entrance. Most of the westward current in the anticyclonic eddy at the lee of the separated GC was recirculated out of the bay and

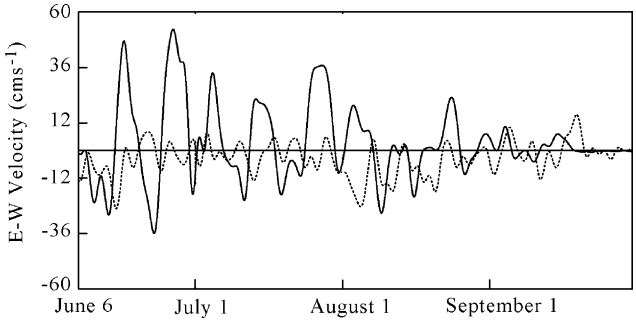

Fig. 7. Time series of E–W velocity component, filtered with a 36 h low-pass filter, at station O1 (depth 20 m, solid curve) and Bonaventure station (depth 7 m, dashed curve) in 1991. Positive values refer to the eastward currents.

had a small impact on the circulation in the central and western parts of the bay. These features are confirmed by the presence of weaker westward currents at the Bonaventure station in June and July (Fig. 7).

Weak mean northwestward and westward currents at O2 in August and September, respectively (Fig. 3c and d) and weak eastward currents at O1 (Fig. 7) in same period imply the existence of the weak separation with a smaller horizontal scale of C_1 limited to the region near the north shore. The corresponding intensified GC intrusion during this period is also indicated by the larger westward currents at the Bonaventure station (Fig. 7). Combined with the results shown in the previous sections, it is clear that the mean circulation patterns in the BdC during these two months resulted from a weaker separation of the GC. Relatively large westward currents shown in the velocity time series at both O1 and Bonaventure station in August and September (Fig. 7) demonstrate the scenario when strong GC intrusion (or weak separation) occurred.

5. Summary

Based on the analysis of data from current meter moorings and CTD profile transects, the summer circulation variability in the BdC is ascribed to the processes of GC intrusion/separation. It is found that strong separation occurred at the entrance of the bay in June and July, likely due to a decelerating GC during this time. A corresponding strong anticyclonic recirculation is formed at the lee of the GC near the entrance of the bay. The circulation in the bay during this time was dominated by a weak GC intrusion. Stronger intrusion occurred in August and September. Larger westward currents intruded into the bay along the north coast, suppressed the prevailing westerly wind stress and formed the cyclonic circulation inside the bay. Thus, it can be concluded that the variability of circulation in the BdC is largely controlled by the intensity of GC separation that is governed by the boundary current dynamics.

Acknowledgements

We thank Paul Peltola, Claude Belanger, S. Lepage, J.C. Croteau and C. Le Quere for help in collecting and processing the data. This work was supported by and is a contribution to the program of the Group Interuniversitaire de Recherche Oceanographiques du Quebec and OPEN (National Center of Excellence in Canada). Funds were also obtained from the Natural Science and Engineering Research Council of Canada (R.G.I.) and the Fonds FCAR (R.G.I.). Authors are grateful to the reviewers for helpful comments.

References

Batchelor, G.K., 1967. An Introduction to Fluid Dynamics. Cambridge University Press, New York, 615 pp.

Benoit, J.M., El-Sabh, I., Tang, C.L., 1985. Structure and seasonal characteristics of the Gaspe current. Journal of Geophysical Research 90 (C2), 3225–3236.

Bonardelli, J.C., Himmelman, J.H., Drinkwater, K., 1993. Current variability and upwelling along the north shore of Baie des Chaleurs. Atmosphere-Ocean 31 (4), 541–565.

Bugden, G.L., 1981. Salt and heat budgets for the Gulf of St. Lawrence. Canadian Journal of Fisheries and Aquatic Sciences 38, 1153–1167.

Filteau, G., Tremblay, J.L., 1953. Ecologie de *Calanus finmarchicus* dans la Baie des Chaleurs. Le Nauraliste Canadien 80, 1–82.

Gan, J.P., Allen, J.S., 2002. A modeling study of shelf circulation off northern California in the region of the coastal ocean dynamics experiments: response to relaxation of upwelling winds. Journal of Geophysical Research 107 (C9), 3123, doi:10.1029/2000JC000768.

Gan, J.P., Ingram, R.G., Greatbatch, R.J., Chen, P., 1995. Upper ocean modelling in a coastal bay. Journal of Geophysical Research 100, 15977–15997.

Gan, J.P., Ingram, R.G., Greatbatch, R.J., 1996. Sensitivity study of upper ocean model in a coastal bay. Journal of Marine System 7, 203–219.

Gan, J.P., Ingram, R.G., Greatbatch, R.J., 1997. On the separation/intrusion of Gaspe current and variability in Baie des Chaleurs, modeling studies. Journal of Geophysical Research 102, 15567–15581.

Lauzier, L.M., Marcotte, A., 1965. Comparaison du climat marin de Grande-Rivière (Baie des Chaleurs) avec celui d'autres stations de la cote atlantique. Journal of the Fisheries Research Board of Canada 22, 1321–1334.

Signell, R.P., Gyer, W.R., 1991. Transient eddy formation around headlands. Journal of Geophysical Research 96, 2561–2575.

Tang, C.L., 1980. Mixing and circulation in the northwestern Gulf of St. Lawrence: a study of a buoyancy-driven current system. Journal of Geophysical Research 85 (C5), 2787–2797.

Wang, D.P., 1987. The straits surface outflow. Journal of Geophysical Research 92, 10807–10825.